Deglacial upwelling, productivity and CO_2 outgassing in the North Pacific Ocean

William R. Gray [1,2]*, James W. B. Rae [2], Robert C. J. Wills [3], Amelia E. Shevenell [4,5], Ben Taylor[2], Andrea Burke [2], Gavin L. Foster[6] and Caroline H. Lear[7]

The interplay between ocean circulation and biological productivity affects atmospheric CO_2 levels and marine oxygen concentrations. During the warming of the last deglaciation, the North Pacific experienced a peak in productivity and widespread hypoxia, with changes in circulation, iron supply and light limitation all proposed as potential drivers. Here we use the boron-isotope composition of planktic foraminifera from a sediment core in the western North Pacific to reconstruct pH and dissolved CO_2 concentrations from 24,000 to 8,000 years ago. We find that the productivity peak during the Bølling–Allerød warm interval, 14,700 to 12,900 years ago, was associated with a decrease in near-surface pH and an increase in pCO_2, and must therefore have been driven by increased supply of nutrient- and CO_2-rich waters. In a climate model ensemble (PMIP3), the presence of large ice sheets over North America results in high rates of wind-driven upwelling within the subpolar North Pacific. We suggest that this process, combined with collapse of North Pacific Intermediate Water formation at the onset of the Bølling–Allerød, led to high rates of upwelling of water rich in nutrients and CO_2, and supported the peak in productivity. The respiration of this organic matter, along with poor ventilation, probably caused the regional hypoxia. We suggest that CO_2 outgassing from the North Pacific helped to maintain high atmospheric CO_2 concentrations during the Bølling–Allerød and contributed to the deglacial CO_2 rise.

The balance between the supply of nutrients and carbon to surface waters via ocean circulation and their removal via biological productivity is a first-order control on atmospheric CO_2. This is particularly important at high latitudes[1,2], where Ekman suction, driven by cyclonic wind stress, and winter mixing supply CO_2 from the deep ocean to the surface. Depending on the availability of light and micronutrients, such as iron, this CO_2 may be captured by photosynthesis and returned to the deep ocean (the 'biological pump'), or may escape to the atmosphere. The balance between circulation and biological productivity is also crucial for determining the ocean's dissolved oxygen content. Ventilation of the ocean at high latitudes mixes oxygen-rich waters from the surface into the ocean's interior, where oxygen is consumed by the respiration of sinking organic matter, coupling the biogeochemical cycles of oxygen and carbon.

Dramatic changes in these biogeochemical balances are thought to occur during Pleistocene deglaciations, with reorganizations of circulation and productivity at high latitudes leading to changes in oceanic oxygen content and rapid atmospheric CO_2 rise[1–4]. However, the degree to which these changes in CO_2 and oxygen are driven by circulation versus biological productivity remains unknown, limiting our understanding of the mechanisms driving glacial–interglacial variations in CO_2 and climate. Particularly enigmatic are the large peaks in productivity observed throughout the North Pacific Ocean during every deglaciation of at least the past approximately million years[5–8]. During the Bølling–Allerød interval (14.7–12.9 thousand years ago) of the last deglaciation (the only deglaciation for which we currently have records of intermediate-ocean redox) the productivity maximum is associated with widespread interme-

diate-ocean hypoxia in the North Pacific[3,9–11]. Since the discovery of these events more than 25 years ago[5,10] multiple explanations have been put forward, yet there is no consensus on the cause of either the productivity or the hypoxia; indeed the degree to which the productivity and hypoxia are linked, and even the direction of causation, are still contested. Some studies have proposed the productivity maximum was caused by an increase in the supply of nutrient- and carbon-rich waters[7,12], while others have suggested alleviation of iron[11,13] and/or light limitation as the main driver[14]. Early work debated the dominance of reduced ventilation versus increased productivity as the primary cause of the hypoxia[9,10], while more recently it has been proposed that hypoxia was initially induced by subsurface warming, and that iron release from hypoxic sediments drove the increase in productivity[11].
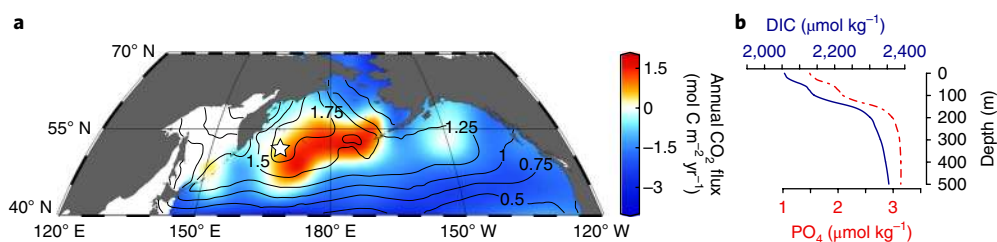
Given the large reservoir of dissolved inorganic carbon (DIC) in the North Pacific interior[15] (Fig. 1), a change in its supply and removal to and from the surface could have significant impact on the global carbon cycle, and play a role in glacial termination. Understanding the nature of these events is also important as they have been suggested to provide insights into future changes in hypoxia and productivity in a rapidly warming climate[3,11].

Boron isotopes and CO_2 supply

To determine the cause of the Bølling–Allerød productivity maximum, we measured the boron isotope composition ($\delta^{11}B$) of the planktic foraminifera *Neogloboquadrina pachyderma* (*N. pachyderma*) from deglacial sediments in core MD01-2416 (51.27° N, 167.73° E, 2,317 m water depth) (Methods). The core site is located close to the centre of the high-nutrient and high-CO_2 pool in the

Fig. 1 | CO₂ and nutrients in the modern subpolar North Pacific. a, Annual surface ocean–atmosphere CO_2 flux[38], with contours of surface ocean phosphate (PO_4) in µmol kg⁻¹ (ref. [39]). The location of core MD01-2416 (51.27° N, 167.73° E, 2,317 m water depth) is indicated by a star. **b**, Upper water column profiles of DIC and phosphate in the western subpolar North Pacific[15].

modern subpolar North Pacific (Fig. 1), making it ideally suited to track changes in the biogeochemistry of the region. δ¹¹B is a proxy for seawater pH, which tracks seawater CO_2 chemistry, and with an estimate of one other parameter of the carbonate system (here alkalinity), allows the quantification of the CO_2 concentration of past seawater[16] (Methods).

Our results show a general decrease in near-surface pH over deglaciation, with a glacial high of 8.31 ± 0.04 (1σ) falling to a value of 8.14 ± 0.04 in the early Holocene, identical to pre-industrial pH at 50 m water depth[15] (Fig. 2). Punctuating the general decline in pH is a pronounced pH minimum of 8.07 ± 0.05 in the early Bølling–Allerød, coeval with the maximum in productivity. At this time, $p\mathrm{CO}_2$ in the near-surface ocean reached a maximum of 373 ± 46 µatm (1σ) (Fig. 3). The decrease in pH and increase in CO_2 demonstrate that the supply of carbon and nutrients to the surface ocean was greater than their removal by export production (Supplementary Fig. 1). As export production during the Bølling–Allerød was higher than today[6,17], it follows that the supply of carbon and macronutrients must also have been higher.

PMIP3 model ensemble and palaeo-circulation tracers

To investigate the physical mechanisms underlying the increase in nutrient and CO_2 supply, we looked for large-scale changes in the PMIP3 model ensemble[18] under glacial boundary conditions, alongside palaeo-tracers of ocean circulation. Although formation of North Pacific Intermediate Water (NPIW) is extremely limited today[19], overturning circulation within the basin was significantly enhanced during the last glacial maximum (LGM): benthic foraminiferal δ¹³C records[20–22] indicate glacial expansion of NPIW to depths of >1500 m (Supplementary Fig. 2), flushing nutrients and carbon from intermediate waters and deepening the interior ocean nutrient/carbon reservoir. North Pacific ventilation may have been even deeper and more vigorous during early deglaciation[23–25], with possible localized deepwater formation during Heinrich Stadial 1[24–26] (HS1) potentially driving the early-deglacial decrease in pH observed in our record (Methods). However, at the onset of the Bølling–Allerød a rapid decrease in benthic δ¹³C and increase in benthic radiocarbon ages indicate a collapse in NPIW formation[23,24], and a circulation more similar to the modern[26] (Fig. 3 and Supplementary Fig. 3).

If the Bølling–Allerød was characterized by similar overturning circulation to today, why was the supply of nutrients and carbon to the surface ocean so much higher? All eight models analysed show substantial increase in wind stress curl within the subpolar gyre under glacial boundary conditions, with an ensemble mean increase of ~60% relative to pre-industrial (Fig. 4). This is driven by the presence of an ice sheet over North America, which causes a strengthening of the westerlies and a southward shift in the polar easterlies, substantially increasing meridional wind shear and associated upwelling by Ekman suction within the subpolar gyre.
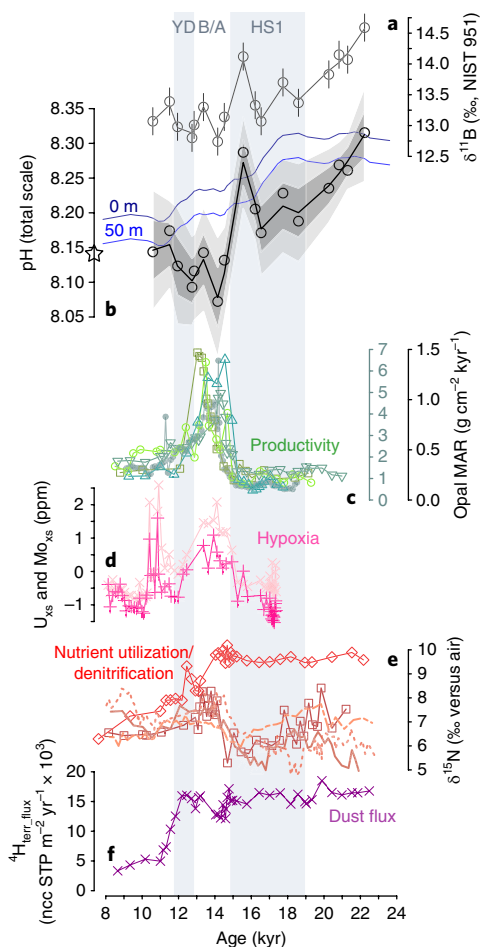
Fig. 2 | Deglacial changes in the biogeochemistry of the subpolar North Pacific. a, δ¹¹B of *N. pachyderma* (versus boric acid standard NIST 951) from MD01-2416. **b**, pH with a LOESS smooth and 1σ and 2σ error envelope (Methods). The star shows pre-industrial pH at this site (50 m water depth) and blue lines show equilibrium pH (Methods). **c**, Opal mass accumulation rate (MAR) from MD01-2416[40] (filled circles, inset-axis), RAMA-PC-44[9] (triangles), PC13[29] (squares), ODP882[41] (open circles) and SO202-07-6[17] (inverse triangles). **d**, Excess U (dark pink) and Mo (light pink) from EW0408-85JC[11,42]. **e**, δ¹⁵N of *N. pachyderma* from SO202-07-6[17] (diamonds), diatoms from PC13[29] (squares), and bulk sediments from MD01-2416[30] (dashed line), ODP887[30] (solid line) and ODP1017[31] (dotted line). **f**, ⁴He flux (ncc STP, nano cubic centimetres at standard temperature and pressure) from SO202-7-6[28]. YD, B/A and HS1 are the Younger Dryas, Bølling–Allerød, and Heinrich Stadial 1. See Supplementary Information for core locations.
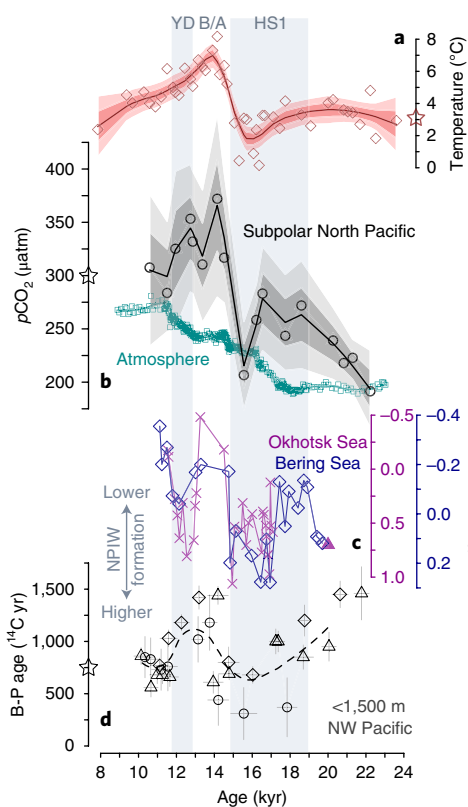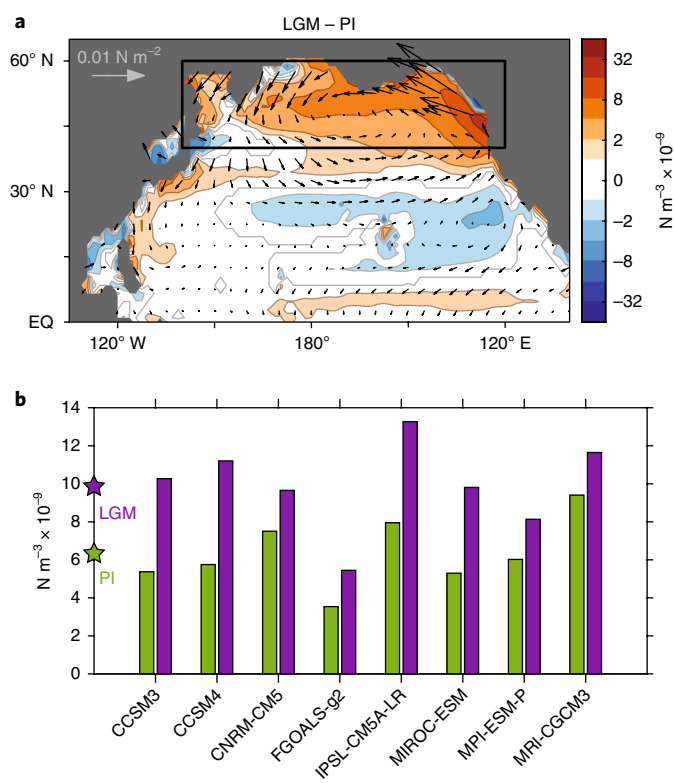
Fig. 3 | Deglacial temperature, pCO_2 and NPIW formation.
a, *N. pachyderma* Mg/Ca-temperature with a LOESS smooth and 1σ and 2σ error envelope. The star shows modern mean annual temperature at the site[39] (50 m water depth). **b**, pCO_2 in the atmosphere[4] and near-surface subpolar North Pacific with a LOESS smooth and 1σ and 2σ error envelope (Methods). The star shows pre-industrial pCO_2 at the site (50 m water depth). **c**, $\delta^{13}C$ of *Cibicidoides* spp. (versus Vienna Pee Dee Belemnite) from the intermediate Bering Sea (SO201-2-85KL) and Okhotsk Sea (SO178-13-6)[23] (Methods). The triangle shows the LGM value for the intermediate-depth (~1,000 m) Okhotsk Sea[20]. **d**, Benthic-planktic (B-P) ^{14}C age difference in the intermediate depth (<1,500 m) northwest Pacific[24] with 1σ error bars and a LOESS smooth; CH84-14 (circles), GH02-1030 (triangles) and MR01K03-PC4/PC5 (diamonds). The star shows pre-bomb benthic-planktic ^{14}C age.

Fig. 4 | Wind stress curl in the glacial North Pacific. a, PMIP3 ensemble mean difference in wind stress curl over the North Pacific in the LGM relative to the pre-industrial (PI) control (positive means greater wind stress curl in the LGM), with changes in vector wind stress indicated by the arrows (see grey arrow in top left corner for scale). The ensemble also includes one PMIP2 model (CCSM3, see Methods). **b**, PI and LGM wind stress curl between 40° N and 60° N (shown by the black box in **a**, corresponding to the position of the subpolar gyre under PI conditions) in each of the models. The ensemble means for the PI and LGM are shown by the stars.

At the onset of the Bølling–Allerød, large ice sheets remained over North America, with the Laurentide Ice Sheet having lost only ~15% of its mass[27]. Ekman suction within the subpolar gyre would therefore have been significantly higher than modern. During the LGM, nutrient flushing by enhanced NPIW formation would have prevented the increase in Ekman suction from increasing the nutrient/carbon supply. However, following the collapse in NPIW at the onset of the Bølling–Allerød, the interior ocean nutrient/carbon reservoir would have shoaled, becoming accessible to the surface ocean (Supplementary Fig. 3). This combination of nutrient- and carbon-rich subsurface waters and enhanced Ekman suction led to a substantial increase in nutrient and carbon supply to the surface.

Nutrient utilization and hypoxia

Higher iron availability from atmospheric dust flux and the alleviation of light-limitation in warm seasonally stratified waters would have also helped Bølling–Allerød productivity to exceed present-day levels[14,28] (Methods). However, our pH and CO_2 record demonstrates that carbon and nutrient supply overwhelmed iron and light availability, leaving a significantly higher proportion of the upwelled macronutrients and carbon unutilized, and reducing the

net efficiency of the biological pump at this location. In contrast to $\delta^{11}B$, foraminiferal $\delta^{15}N$ shows little change at the onset of the Bølling–Allerød productivity maximum[17,29,30] (Fig. 2). While no change in $\delta^{15}N$ during an increase in productivity is consistent with an increase in nutrient supply[17], previous interpretations have suggested increased nutrient supply was balanced by higher export production, such that there was no net change in the efficiency of the biological pump[17]. However, $\delta^{15}N$ is also influenced by the isotopic composition of source water nitrate, which is thought to have increased at the Bølling–Allerød due to enhanced denitrification associated with regional hypoxia[29–32] (Fig. 2). Signals of reduced nutrient utilization at the Bølling–Allerød are thus likely to be somewhat masked or delayed in $\delta^{15}N$ records (Methods).

The increase in export production during the Bølling–Allerød would have increased organic matter respiration, consuming oxygen in the ocean's interior. The supply of oxygen to intermediate waters would also have been reduced, due to the collapse in NPIW formation. Both processes thus contributed to the regional hypoxia observed at this time. The initiation of hypoxia may have acted as a positive feedback on productivity by increasing iron concentrations within upwelling waters[11], but it was not the primary cause of the increase in productivity.

Deglacial CO2 rise

The increase in pCO_2 within the near-surface ocean at the onset of the Bølling–Allerød would have resulted in significant outgassing

of CO_2, with our reconstructed ocean–atmosphere pCO_2 difference being ~130 µatm. Although *N. pachyderma* calcifies at around 50 m water depth (Methods) the average annual pCO_2 difference between 50 m depth and the surface ocean is only ~10 µatm at the core site today, thus the surface ocean would have also experienced elevated levels of CO_2 (Methods). A significant release of CO_2 is also supported by the warm temperatures recorded by the Mg/Ca of *N. pachyderma* during this time (Fig. 3), which, as well as indicating a relatively near-surface habitat, would also have helped drive CO_2 outgassing from the ocean to atmosphere (Methods). Release of CO_2 from the subpolar Pacific at the onset of the Bølling–Allerød may have contributed to the rapid ~10 µatm increase in atmospheric CO_2 observed at this time[4,12] (Fig. 3; Methods). Furthermore, continued CO_2 outgassing from the North Pacific would have maintained the high levels of atmospheric pCO_2 observed throughout the Bølling–Allerød, countering the return to more stratified conditions in the Southern Ocean[4,16,33,34] and the ventilation of the Atlantic with low preformed nutrient NADW[35], both of which should drive down atmospheric pCO_2. The upwelling of CO_2-rich waters in the North Pacific may thus allow atmospheric pCO_2 to stay high—rather than falling—during the Bølling–Allerød, and help drive continued deglaciation.

Results from ocean drilling in the Bering Sea indicate an expansion of NPIW during every glacial period of the past 1.2 million years[36]. All that is required for the model proposed here to explain the regular deglacial North Pacific productivity peaks is that the switch from the enhanced glacial mode of NPIW formation to the reduced interglacial mode precedes the loss of the Laurentide Ice Sheet and its associated enhanced Ekman suction. Brine rejection within the Bering Sea has been suggested as an important process by which NPIW formation was enhanced during glacial periods[36]. Over the last deglaciation there was an almost total loss of sea ice within the Bering Sea following the Northern Hemisphere warming at the Bølling–Allerød[37]; however, the Laurentide Ice Sheet did not ablate completely until ~7,000 years later[27]. If the expansion of NPIW during glacial periods is driven by enhanced brine rejection, then the loss of sea ice prior to ice sheets during deglacial warming would dictate that increased upwelling of carbon- and nutrient-rich waters—and associated CO_2 release—would regularly occur during glacial terminations.

Methods

Methods, including statements of data availability and any associated accession codes and references, are available at https://doi.org/10.1038/s41561-018-0108-6.

References

1. Toggweiler, J. R. Variation of atmospheric CO_2 by ventilation of the ocean's deepest water. *Paleoceanography* **14**, 571–588 (1999).
2. Sigman, D. M., Hain, M. P. & Haug, G. H. The polar ocean and glacial cycles in atmospheric CO_2 concentration. *Nature* **466**, 47–55 (2010).
3. Jaccard, S. L. & Galbraith, E. D. Large climate-driven changes of oceanic oxygen concentrations during the last deglaciation. *Nat. Geosci.* **5**, 151–156 (2011).
4. Marcott, S. A. et al. Centennial-scale changes in the global carbon cycle during the last deglaciation. *Nature* **514**, 616–619 (2014).
5. Keigwin, L., Jones, G. A. & Froelich, P. N. A 15,000 year paleoenvironmental record from Meiji Seamount, far northwestern Pacific. *Earth Planet. Sci. Lett.* **111**, 425–440 (1992).
6. Kohfeld, K. E. & Chase, Z. Controls on deglacial changes in biogenic fluxes in the North Pacific Ocean. *Quat. Sci. Rev.* **30**, 3350–3363 (2011).
7. Jaccard, S. L. et al. Glacial/interglacial changes in subarctic North Pacific stratification. *Science* **308**, 1003–1006 (2005).
8. Jaccard, S. L., Galbraith, E. D., Sigman, D. M. & Haug, G. H. A pervasive link between Antarctic ice core and subarctic Pacific sediment records over the past 800kyrs. *Quat. Sci. Rev.* **29**, 206–212 (2010).
9. Crusius, J., Pedersen, T. F., Kienast, S., Keigwin, L. & Labeyrie, L. Influence of northwest Pacific productivity on North Pacific Intermediate Water oxygen concentrations during the Bølling–Allerød interval (14.7–12.9 ka). *Geology* **32**, 633–636 (2004).
10. Behl, R. J. & Kennett, J. P. Brief interstadial events in the Santa Barbara basin, NE Pacific, during the past 60 kyr. *Nature* **379**, 243–245 (1996).
11. Praetorius, S. K. et al. North Pacific deglacial hypoxic events linked to abrupt ocean warming. *Nature* **527**, 362–366 (2015).
12. Galbraith, E. D. et al. Carbon dioxide release from the North Pacific abyss during the last deglaciation. *Nature* **449**, 890–893 (2007).
13. Mix, A. C. et al. in *Mechanisms of Global Climate Change at Millennial Time Scales* (eds Clark, P. U. et al.) 127–148 (American Geophysical Union, Washington, DC, 1999).
14. Lam, P. J. et al. Transient stratification as the cause of the North Pacific productivity spike during deglaciation. *Nat. Geosci.* **6**, 622–626 (2013).
15. Key, R. M. et al. *Global Ocean Data Analysis Project* Version 2 (GLODAPv2) ORNL/CDIAC-162 (US Department of Energy, 2015); https://doi.org/10.3334/CDIAC/OTG.NDP093_GLODAPv2
16. Martínez-Botí, M. A. et al. Boron isotope evidence for oceanic carbon dioxide leakage during the last deglaciation. *Nature* **518**, 219–222 (2015).
17. Ren, H. et al. Glacial-to-interglacial changes in nitrate supply and consumption in the subarctic North Pacific from microfossil-bound N isotopes at two trophic levels. *Paleoceanography* **30**, 1217–1232 (2015).
18. Braconnot, P. et al. Evaluation of climate models using palaeoclimatic data. *Nat. Clim. Chang.* **2**, 417–424 (2012).
19. Talley, L. D. Distribution and formation of North Pacific intermediate water. *J. Phys. Oceanogr.* **23**, 517–537 (1993).
20. Keigwin, L. Glacial age hydrography of the far northwest Pacific Ocean. *Paleoceanography* **13**, 323–339 (1998).
21. Max, L. et al. Evidence for enhanced convection of North Pacific Intermediate Water to the low-latitude Pacific under glacial conditions. *Paleoceanography* **32**, 41–55 (2017).
22. Matsumoto, K., Oba, T. & Lynch-Stieglitz, J. Interior hydrography and circulation of the glacial Pacific Ocean. *Quat. Sci. Rev.* **21**, 1693–1704 (2002).
23. Max, L. et al. Pulses of enhanced North Pacific Intermediate Water ventilation from the Okhotsk Sea and Bering Sea during the last deglaciation. *Clim. Past.* **10**, 591–605 (2014).
24. Okazaki, Y. et al. Deepwater formation in the North Pacific during the last glacial termination. *Science* **329**, 200–204 (2010).
25. Rae, J. W. B. et al. Deep water formation in the North Pacific and deglacial CO_2 rise. *Paleoceanography* **29**, 645–667 (2014).
26. Cook, M. S. & Keigwin, L. Radiocarbon profiles of the NW Pacific from the LGM and deglaciation: evaluating ventilation metrics and the effect of uncertain surface reservoir ages. *Paleoceanography* **30**, 174–195 (2015).
27. Ullman, D. J., Carlson, A. E., Anslow, F. S., LeGrande, A. N. & Licciardi, J. M. Laurentide ice-sheet instability during the last deglaciation. *Nat. Geosci.* **8**, 534–537 (2015).
28. Serno, S. et al. Comparing dust flux records from the Subarctic North Pacific and Greenland: Implications for atmospheric transport to Greenland and for the application of dust as a chronostraphic tool. *Paleoceanography* **30**, 583–600 (2015).
29. Brunelle, B. G. et al. Glacial/interglacial changes in nutrient supply and stratification in the western subarctic North Pacific since the penultimate glacial maximum. *Quat. Sci. Rev.* **29**, 2579–2590 (2010).
30. Galbraith, E. D. et al. Consistent relationship between global climate and surface nitrate utilization in the western subarctic Pacific throughout the last 500 ka. *Paleoceanography* **23**, PA2212 (2008).
31. Hendy, I. L., Pedersen, T. F., Kennett, J. P. & Tada, R. Intermittent existence of a southern Californian upwelling cell during submillennial climate change of the last 60 kyr. *Paleoceanography* **19**, PA3007 (2004).
32. Deutsch, C., Sigman, D. M., Thunell, R. C., Meckler, A. N. & Haug, G. H. Isotopic constraints on glacial/interglacial changes in the oceanic nitrogen budget. *Glob. Biogeochem. Cycles* **18**, GB4012 (2004).
33. Anderson, R. F. et al. Wind-driven upwelling in the Southern Ocean and the deglacial rise in atmospheric CO_2. *Science* **323**, 1443–1448 (2009).
34. Burke, A. & Robinson, L. F. The Southern Ocean's role in carbon exchange during the last deglaciation. *Science* **335**, 557–561 (2012).
35. McManus, J. F., Francois, R., Gherardi, J. M. & Keigwin, L. Collapse and rapid resumption of Atlantic meridional circulation linked to deglacial climate changes. *Nature* **428**, 834–837 (2004).
36. Knudson, K. P. & Ravelo, A. C. North Pacific Intermediate Water circulation enhanced by the closure of the Bering Strait. *Paleoceanography* **30**, PA002840 (2015).
37. Mheust, M., Stein, R., Fahl, K., Max, L. & Riethdorf, J.-R. High-resolution IP25-based reconstruction of sea-ice variability in the western North Pacific and Bering Sea during the past 18,000 years. *Geo. Mar. Lett.* **36**, 101–111 (2015).

38. Takahashi, T. et al. Climatological mean and decadal change in surface ocean $p\text{CO}_2$, and net sea-air CO_2 flux over the global oceans. *Deep. Sea Res. II* **56**, 554–577 (2009).
39. Boyer, T. P. et al. *World Ocean Database 2013*. *NOAA Atlas NESDIS 72* (eds Leviticus, S. & Mishonov, A.) 209 (NOAA, Silver Spring, 2013)
40. Gebhardt, H. et al. Paleonutrient and productivity records from the subarctic North Pacific for Pleistocene glacial terminations I to V. *Paleoceanography* **23**, PA4212 (2008).
41. Jaccard, S. L. et al. Subarctic Pacific evidence for a glacial deepening of the oceanic respired carbon pool. *Earth Planet. Sci. Lett.* **277**, 156–165 (2009).
42. Barron, J. A., Bukry, D., Dean, W. E., Addison, J. A. & Finney, B. Paleoceanography of the Gulf of Alaska during the past 15,000 years: results from diatoms, silicoflagellates, and geochemistry. *Mar. Micro.* **72**, 176–195 (2009).

Author contributions

W.R.G. and J.W.B.R. designed the study and wrote the manuscript. W.R.G., J.W.B.R, G.L.F., C.H.L., B.T. and A.E.S. were involved in the generation of the trace element and $\delta^{11}\text{B}$ data; R.C.J.W. analysed climate model output; all authors contributed to the interpretation and preparation of the final manuscript.

Competing interests

The authors declare no competing interests.

Additional information

Supplementary information is available for this paper at https://doi.org/10.1038/s41561-018-0108-6.

Reprints and permissions information is available at www.nature.com/reprints.

Correspondence and requests for materials should be addressed to W.R.G.

Publisher's note: Springer Nature remains neutral with regard to jurisdictional claims in published maps and institutional affiliations.

Methods

Habitat depth and seasonality of *N. pachyderma* in the western North Pacific.
Sediment trap data in the modern northwest Pacific display two seasonal
N. pachyderma abundance peaks during the spring and autumn, roughly
corresponding to the time of most, and least, stratification, respectively. As these
fluxes are more or less equal, the geochemical signature of *N. pachyderma* should
represent mean annual oceanographic conditions at a water depth of ~50 m (ref. [43]),
provided that the growing season of *N. pachyderma* did not change substantially in
the past.

Core materials. Core MD01-2416 was raised from 51.27° N, 167.73° E, 2,317 m
water depth on the Detroit Seamount. This site is situated within the subpolar
North Pacific High Nutrient Low Chlorophyll zone, making it well suited to
track past changes in CO_2 outgassing in this region (Fig. 1). %Opal data from
the core (Fig. 2) were previously published (refs [40,44]), and were converted into
mass accumulation rate using the age model described below. Foraminifera are
well-preserved throughout the deglaciation in this core, likely due to its high
sedimentation rate and the relatively muted changes in carbonate ion since the
LGM in the deep Pacific[45].

Age model for MD01-2416. We generated a new age model for the core by
recalibrating 36 *N. pachyderma* [14]C dates from ref. [46], excluding 6 ^{14}C dates
previously demonstrated to show evidence of reworking[46]. The ^{14}C dates were
calibrated with INTCAL13[47]. There are likely to be considerable changes in
deglacial reservoir age which are difficult to constrain; we apply a constant
reservoir age of 950 ± 450 yrs, which encompasses the modern seasonal variability
within the region, as well as palaeo-reconstructions and model estimates for the
LGM, deglaciation and the Holocene[48–51]. The age model was constructed using the
BACON[52] Bayesian age modelling package in R. Uncertainty in calibrated age is
typically ±800 years at the 95% confidence interval, increasing to greater than
±1,000 years before ~21 kyr ago. Using the ^{14}C plateau-tuned chronology of ref. [46]
makes no difference to any of the conclusions drawn (Supplementary Fig. 4).

δ^{11}B and trace element analysis. Well-preserved *N. pachyderma* were picked
from the 150–250 µm size fraction at a 3–15 cm resolution. Approximately 400
individuals were used per δ^{11}B analysis. Samples were cleaned in a class 100 clean
lab at the National Oceanography Centre Southampton (NOCS) according to the
'Mg' method of ref. [53] as detailed in ref. [54]. A ~5% split of the cleaned foraminiferal
samples was analysed after acidification for a suite of trace elements at NOCS using
an Element II HR-ICP-MS against matrix-matched standards. δ^{11}B was analysed at
NOCS on a Neptune MC-ICP-MS following the method of ref. [54,55], which involves
removing the sample matrix prior to analysis using anionic exchange resin, and
sample-standard bracketing to correct for instrument-induced mass fractionation.
Long-term reproducibility of this approach is ±0.23‰ at the 95% confidence
interval[56].

To increase the resolution of the Mg/Ca record, 26 additional samples were
analysed for trace elements only. Between 20 and 50 individual *N. pachyderma*
were cleaned following the oxidative/reductive protocol of ref. [57]. The samples were
analysed at Cardiff University using an Element II HR-ICP-MS against matrix-
matched standards. The same standards were used at both Cardiff University and
NOCS to ensure consistency.

Average Al/Ca values are ~50 µmol mol^{−1}. Six samples have Al/Ca in the range
100–150 µmol mol^{−1}; however, these samples do not display elevated Mg/Ca
or B/Ca, indicating no influence of clay contamination. Average Mn/Ca for
samples cleaned using the 'Mg' method is 80 µmol mol^{−1}, whereas average Mn/Ca
for reductively cleaned samples is <10 µmol mol^{−1}. Despite the higher Mn/Ca
values of the 'Mg' cleaned samples, both data sets display very similar Mg/Ca
(after correction for preferential dissolution of high-Mg calcite during reductive
cleaning[53]) and B/Ca values downcore, indicating no influence of Mn-Fe
oxyhydroxide coatings. Previously published Mg/Ca data from MD01-2416[40,44]
show elevated values compared to the data cleaned by both the 'Mg' method
and the reductive method in this study, indicating a possible influence of
contamination, so are not used in our temperature reconstruction. Including these
data makes no difference to any of the conclusions drawn.

Temperature record. The Mg/Ca values were converted to temperature using the
species-specific calibration of ref. [58] (recalculated by ref. [59]). Samples that had been
reductively cleaned were adjusted upwards by 12.5% to account for preferential
dissolution of high-Mg calcite during reductive cleaning[53]. The data were fitted
with a non-parametric regression (LOESS) in R. The smoothing parameter (α) was
optimized using generalized cross validation (GCV). A Monte Carlo approach was
used to determine the most likely fit to the data, with the LOESS smooth fitted to
ten thousand realizations of the temperature data with an uncertainty of ± 2.3 °C
(2σ), accounting for the 1.2 °C (2σ) calibration error[58], and incorporating terms
for uncertainty in salinity (±2 practical salinity units (PSU) [2σ] with a sensitivity
of 3% per PSU unit[60,61]) and pH (±0.2 pH units [2σ] with a sensitivity of −7% per
0.1 pH unit[61,62]).

pH is known to affect planktic foraminiferal Mg/Ca with a sensitivity of
approximately −7% per 0.1 pH unit[61,62]. While the pH minimum during the

Bølling–Allerød may be influencing the apparent Mg/Ca temperatures, this
influence is likely to be minimal. Firstly, as the absolute value of pH during the
Bølling–Allerød is broadly equivalent to pre-industrial (it is a large
anomaly from equilibrium due to lower atmospheric CO_2 concentrations during
the Bølling–Allerød) the effect of pH on absolute temperature will be negligible.
Secondly, the ΔpH at the onset of the Bølling–Allerød is ~0.15 units, so given
a Mg/Ca sensitivity of −7% per 0.1 pH unit, this could only account for a 10%
increase in Mg/Ca, or ~1–1.5 °C, considerably smaller than the ~5 °C warming
indicated by the Mg/Ca record at the onset of the Bølling–Allerød. The effect
of higher pH during the LGM means our Mg/Ca temperature record is likely to
be underestimating LGM temperature by ~1–1.5 °C. Dissolution can also affect
foraminiferal Mg/Ca, although this influence is relatively minor in lower-Mg
planktic foraminifera such as *N. pachyderma*[63]. LGM–Holocene changes in
bottom water carbonate ion concentration are also relatively minor within the
Pacific (~10 µmol kg^{−1})[45], and our Mg/Ca data show no correlation with %CaCO₃
in this core, so dissolution is unlikely to have a significant influence on our
record. Our temperature record shows good agreement with the assemblage-
derived temperature record of refs [40,44] from the same core. Recent research found
that the *Globigerinoides ruber* Mg/Ca-temperature sensitivity is lower than the
widely applied 9% °C[−1] temperature sensitivity[61]; if future calibration work also
demonstrates similar results for *N. pachyderma*, our Mg/Ca-temperature record
may need minor revision.

Carbonate system calculations. To calculate pH the δ^{11}B of *N. pachyderma* was
converted to seawater δ^{11}B$_{borate}$ using the calibration of ref. [64], where δ^{11}B$_{borate}$ =
δ^{11}B$_{Npachyderma}$ + 3.38 ± 0.71‰ (2σ). To fully explore the uncertainty associated with
the calibration, we recalibrated the data set of ref. [64], varying the slope between
0.6 and 1.4 (which incorporates the range previously observed in all other species
of planktic foraminifera; refs [16,65,66]) with a flat probability distribution, allowing
the intercept to vary (see sensitivity test below). pH was calculated from δ^{11}B$_{borate}$
using a seawater δ^{11}B value[67] of 39.61‰ and the experimentally determined
fractionation factor[68] of 1.0272 following ref. [69]. The boric acid dissociation
constant (K_B) was calculated with the Mg/Ca temperature, and an estimate
of salinity generated by taking the salinity at the site today (33.0 PSU), and
accounting for the whole ocean change in salinity over deglaciation by scaling the
1.15 PSU glacial salinity increase of ref. [70] to the sea level curve of ref. [71]. To fully
propagate uncertainty in reconstructed pH a Monte-Carlo approach was taken,
with ten thousand realizations of the data accounting for the uncertainties in the
measurement of δ^{11}B$_{Npachyderma}$, the conversion of the δ^{11}B$_{Npachyderma}$ to δ^{11}B$_{borate}$, and
of the uncertainty in the temperature and salinity reconstructions on K_B using the
confidence interval of the LOESS temperature smooth and a salinity uncertainty
of ±2 units (2σ). Typical uncertainty on the pH reconstruction following this
approach is ±0.084 (2σ), which is chiefly due to the uncertainty in the offset
between the δ^{11}B of *N. pachyderma* and seawater δ^{11}B$_{borate}$ (±0.078; 2σ). Using
a constant value of K_B (that is, constant temperature and salinity) has no major
influence on reconstructed pH values (see sensitivity test). Preservation has not
been shown to influence planktic δ^{11}B (ref. [72])

An additional parameter of the carbonate system is required to calculate pCO_2
from pH, and total alkalinity is widely used[16,55,64]. Although modelling studies can
provide estimates of the change in alkalinity during the LGM[1,73], there are few
data-based constraints on its secular evolution over deglaciation. Here we follow
the approach of ref. [16], taking a range in alkalinity between modern-day alkalinity at
the site (2,235 µmol kg^{−1}) plus an estimate of the glacial alkalinity increase based on
the modelling results of refs [1,73] (+125 µmol kg^{−1}), and modern-day alkalinity at the
site minus 25 µmol kg^{−1}, with a 'flat' probability distribution between these values.
With this approach there is an equal probability of total alkalinity being at any
value between 2,210 and 2,360 µmol kg^{−1} at any point in the record, fully exploring
the likely range in alkalinity without giving weight to any particular value. Note,
this range in alkalinity is cautious, being broadly equivalent to the range observed
across the surface of the entire open Pacific Ocean today. The pCO_2 of seawater
was calculated using the *seacarb* package in R[74], using the constants of refs [75–77].
To fully propagate the uncertainty associated with each parameter, ten thousand
realizations of pH, total alkalinity, temperature and salinity were input, using the
uncertainty on each parameter described above. Following this approach, the total
uncertainty associated with our pCO_2 estimates is typically ±64 µatm (2σ), which
again is chiefly due to the uncertainty in the offset between δ^{11}B$_{Npachyderma}$ and δ
[11]B$_{borate}$ (±55 µatm). pCO_2 estimates are almost entirely driven by the pH estimates
(Supplementary Fig. 5). Typical pCO_2 uncertainty associated with the temperature
uncertainty is ±2 µatm (2σ), and the uncertainty associated with the salinity
uncertainty is ±10 µatm (2σ). Using either a constant 'modern minus 25 µmol kg^{−1}'
or 'modern plus 125 µmol kg^{−1}' total alkalinity changes the pCO_2 values by only
±20 µatm.

Surface ocean pH at equilibrium with the atmosphere was calculated using
alkalinity calculated in the manner described above, and the atmospheric CO_2
record of ref. [4]. Salinity (estimated in the manner described above) and Mg/Ca
temperature were used to constrain changes in dissociation constants. Equilibrium
pH at 50 m is calculated by applying the modern surface–50m pH gradient
(−0.035 units); deviations from equilibrium pH therefore represent changes in the
carbonate system beyond those expected from changing atmospheric CO_2.

Both the pH and pCO$_2$ records were fitted with a LOESS smooth in R, with the smoothing parameter (α) determined by GCV. To determine the most likely fit to the data a LOESS smooth fitted to ten thousand realizations of the data, accounting for the uncertainties in the pH and pCO$_2$ estimates in the manner described above; this approach allows us to identify significant trends within the data and reduce uncertainty in our estimates.

Carbonate system sensitivity tests. As the current $\delta^{11}B_{calcite}$–$\delta^{11}B_{borate}$ calibration for *N. pachyderma* comes from a limited range in pH[64], application of this calibration to the northwest Pacific requires extrapolation beyond the calibrated range. We tested the sensitivity of our results to the assumed slope of calibration, building on the test outlined in ref.[78]. We re-calibrated the coretop data of ref.[64], forcing the slope within the range previously observed in all other species of planktic foraminifera (refs[16,65,66]), while allowing the intercept to vary (Supplementary Fig. 6). This exercise demonstrates that within the range previously observed in all other species of planktic foraminifera, the assumed slope of the $\delta^{11}B_{calcite}$–$\delta^{11}B_{borate}$ calibration makes no difference to any of the conclusions drawn in this study.

To provide a further constraint on the relationship between $\delta^{11}B_{Npachyderma}$ and $\delta^{11}B_{borate}$, we measured the $\delta^{11}B$ of *N. pachyderma* (following the method described above) from Holocene sediments in core MD02-2489 (54.39° N, 148.92° E, 3,640 m water depth), located in the eastern subpolar Pacific, where modern pH values are significantly higher than in the western subpolar Pacific. Comparing this data along with the Holocene $\delta^{11}B_{Npachyderma}$ data from site MD01-2416 to pre-industrial $\delta^{11}B_{borate}$ (calculated from ref.) shows excellent agreement with the *N. pachyderma* $\delta^{11}B_{calcite}$–$\delta^{11}B_{borate}$ calibration proposed by ref.[64] over a range of $\delta^{11}B$ approximately equivalent to our down-core reconstruction (Supplementary Fig. 6).

To test the sensitivity of our pH and pCO$_2$ reconstructions to temperature, we calculated pH and pCO$_2$ assuming constant temperatures of 2 °C, 5 °C and 8 °C (broadly the deglacial range suggested by the Mg/Ca). Supplementary Fig. 7 demonstrates that using a constant temperature in our carbonate system calculations would not have any effect on the main findings of this study. Compiling all available proxy temperature data in the western subpolar North Pacific demonstrates that using the reconstructed temperatures suggested by all available proxies (Mg/Ca, U$^{k'}_{37}$, TEX$_{86}$, foraminiferal assemblage transfer function; refs[40,79–81]) in our carbonate system calculations results in a substantial outgassing of CO$_2$ from the subpolar North Pacific during the Bølling–Allerød.

Overturning and CO$_2$ in early deglaciation. In addition to the large decrease in pH at the onset of the Bølling–Allerød, our record demonstrates a decrease in pH during early deglaciation, reaching a minimum in HS1. Benthic foraminiferal δ^{13}C and radiocarbon records show an increase in overturning circulation during early deglaciation relative to the LGM[23,24], with possible local deepwater formation during HS1[24,25] (Supplementary Fig. 8). The deepening of the overturning circulation during early-deglaciation would have allowed deeply sequestered nutrients and CO$_2$ to mix more vigorously through the water column[25], resulting in the observed decrease in pH and increase in CO$_2$ in the near-surface ocean, and outgassing of CO$_2$ to the atmosphere. The increase in overturning would have resulted in a deepening of the mixed layer, such that light may have become limiting to primary production[14]. A return to a shallower overturning circulation (similar to the LGM) during late-HS1 would have lessened the upward mixing of deep carbon, increasing pH. Note, removing the high-pH data point at ~15.5 kyr ago makes no difference to any of the conclusions drawn in this study; even without this high-pH data point there is a ~0.1 pH unit decrease from the mean HS1 value going into the Bølling–Allerød, indicating a substantial increase in nutrient and CO$_2$ supply.

Nutrient utilization/denitrification controls on δ^{15}N. Nitrogen isotope records may be influenced by both the degree of nitrate utilization and the isotopic composition of nitrate in the source water[29,30,32,82,83]. The widespread hypoxia accompanying the Bølling–Allerød productivity maximum is thought to have significantly increased denitrification in the oxygen minimum zones of the northeast Pacific[29,31,82,83], driving up the δ^{15}N of seawater nitrate. This is reflected by the large increase in bulk sediment δ^{15}N in cores from the Mexican[82] and Californian[31] continental margins to the Alaskan gyre[30] (Fig. 2). This signal is spread throughout the subsurface North Pacific[30], influencing the δ^{15}N of nitrate upwelled in the northwest Pacific. Records of δ^{15}N from the northwest Pacific (including bulk-sediment, diatom-bound and foram-bound δ^{15}N) show relatively muted changes at the onset of the Bølling–Allerød[17,29,30]. This likely reflects the opposing influences of a decrease in nutrient utilization, due to higher nutrient supply in this key upwelling region, and the increase in δ^{15}N of source water nitrate due to hypoxia-driven denitrification.

Constraints on CO$_2$ uptake within the mixed layer. CO$_2$ concentrations in the mixed layer are likely to be lower than at the ~50 m depth habitat of *N. pachyderma*. However, the mean annual difference between 50 m and surface ocean at this core site today is only ~10 µatm. During the summer months this difference is 21.9 µatm (ref.), due to export production from the mixed layer, and during winter is close to zero, due to mixing of the upper water column. While it is possible this difference was higher in the past, the Mg/Ca of the *N.*

pachyderma indicates temperatures of 5–7 °C during the interval of low pH/high CO$_2$, suggesting that the *N. pachyderma* are recording a signal close to the surface at this time, the mixed layer was deeper and thus thermal stratification weak, or the *N. pachyderma* are recording a summer signal at this time, which would make the CO$_2$ concentrations a minimum estimate. All of these scenarios would result in a significant flux of CO$_2$ to the atmosphere.

CO$_2$ outgassing and atmospheric CO$_2$ change. Net changes in atmospheric CO$_2$ on millennial timescales are strongly influenced by the inventory of preformed versus remineralized nutrients in the ocean's interior[73,84]. Constraining preformed nutrient inventory is challenging using palaeo-proxies. However, given the increased nutrient consumption[17] and high pH/low CO$_2$ of the near-surface North Pacific during the LGM (Figs. 1 and 2), glacial NPIW would likely have had lower preformed nutrient content than the water in the upper 1,500 m of the North Pacific today[85]. Overall this would make the biological pump more efficient at the LGM, driving down atmospheric CO$_2$. At the onset of the Bølling–Allerød, our data suggest a net weakening in the strength of the North Pacific biological pump and substantial outgassing of CO$_2$ from near-surface waters. The collapse in NPIW formation at this time would also have removed this source of relatively low preformed nutrient water from the ocean's interior, and thus would also act to increase atmospheric CO$_2$.

Benthic δ^{13}C records. The benthic δ^{13}C records (*Cibicidoides* spp.) were corrected for the whole ocean change in δ^{13}C relating to changes in the terrestrial biosphere by scaling the value of ref.[86] to global sea level[71]. This only affects the long-term trend, and makes no difference to millennial-scale events within the records.

PMIP3 model output. We analyse the difference in North Pacific wind-stress curl between LGM and pre-industrial conditions as represented by eight coupled climate models (listed in Fig. 4b). All models but CCSM3 are part of the Coupled Model Intercomparison Project phase 5 (CMIP5). Orbital parameters, atmospheric greenhouse gas concentrations, coastlines and ice topography for the LGM simulations are standardized as part of the Paleoclimate Model Intercomparison Project phase 3 (PMIP3) and represent best estimates of the climate state at the LGM, 21 kyr before present[10]. We include data from comparable LGM and pre-industrial simulations[87,88] using an older model, CCSM3, used extensively in palaeoclimate studies. We compute the wind stress curl climatology based on the atmospheric output of each model. The computed wind stress curl is linearly interpolated onto a common grid to compute the ensemble mean (Fig. 4a). Individual model results are shown on Supplementary Figure 9.

Data availability. The authors declare that data supporting the findings of this study are available within the article and its supplementary information files. Data are also available on *Pangaea* (https://doi.pangaea.de/10.1594/PANGAEA.887381).

References

43. Kuroyanagi, A., Kawahata, H. & Nishi, H. Seasonal variation in the oxygen isotopic composition of different-sized planktonic foraminifer *Neogloboquadrina pachyderma* (sinistral) in the northwestern North Pacific and implications for reconstruction of the paleoenvironment. *Paleoceanography* **26**, PA4215 (2011).
44. Sarnthein, M. et al. Mid Holocene origin of the sea-surface salinity low in the subarctic North Pacific. *Quat. Sci. Rev.* **23**, 2089–2099 (2004).
45. Yu, J. et al. Responses of the deep ocean carbonate system to carbon reorganization during the last glacial-interglacial cycle. *Quat. Sci. Rev.* **76**, 39–52 (2013).
46. Sarnthein, M., Schneider, B. & Grootes, P. M. Peak glacial ^{14}C ventilation ages suggest major draw-down of carbon into the abyssal ocean. *Clim. Past.* **9**, 2595–2614 (2013).
47. Reimer, P. J. et al. IntCal13 and Marine13 radiocarbon age calibration curves 0-50,000 years cal BP. *Radiocarbon* **55**, 1869–1887 (2013).
48. Takahashi, T., Olafsson, J., Goddard, J. G., Chipman, D. W. & Sutherland, S. C. Seasonal variation of CO$_2$ and nutrients in the high-latitude surface oceans: a comparative study. *Glob. Biogeochem. Cycles* **7**, 843–878 (1993).
49. Butzin, M., Prange, M. & Lohmann, G. Readjustment of glacial radiocarbon chronologies by self-consistent three-dimensional ocean circulation modeling. *Earth Planet. Sci. Lett.* **317-318**, 177–184 (2012).
50. Kovanen, D. J. & Easterbrook, D. J. Paleodeviations of radiocarbon marine reservoir values for the northeast Pacific. *Geology* **30**, 243–246 (2002).
51. Southon, J. R., Nelson, D. E. & Vogel, J. S. A record of past ocean–atmosphere radiocarbon differences from the northeast Pacific. *Paleoceanography* **5**, 197–206 (1990).
52. Blaauw, M. & Christen, J. A. Flexible paleoclimate age-depth models using an autoregressive gamma process. *Bayesian Anal.* **6**, 457–474 (2011).
53. Barker, S., Greaves, M. & Elderfield, H. A study of cleaning procedures used for foraminiferal Mg/Ca paleothermometry. *Geochem. Geophys. Geosyst.* **4**, 8407 (2003).

54. Rae, J. W. B., Foster, G. L., Schmidt. N.. & Elliott T.. Boron isotopes and B/Ca in benthic foraminifera: proxies for the deep ocean carbonate system. *Earth Planet. Sci. Lett.* **302**, 403–413 (2011).

55. Foster, G. L. Seawater pH, pCO2 and [CO32-] variations in the Caribbean Sea over the last 130 kyr: a boron isotope and B/Ca study of planktic foraminifera. *Earth Planet. Sci. Lett.* **271**, 254–266 (2008).

56. Foster, G. L. et al. Interlaboratory comparison of boron isotope analyses of boric acid, seawater and marine CaCO₃ by MC-ICPMS and NTIMS. *Chem. Geol.* **358**, 1–14 (2013).

57. Boyle, E. A. & Keigwin, L. Comparison of Atlantic and Pacific paleochemical records for the last 215,000 years: changes in deep ocean circulation and chemical inventories. *Earth Planet. Sci. Lett.* **76**, 135–150 (1985).

58. Elderfield, H. & Ganssen, G. Past temperature and δ18O of surface ocean waters inferred from foraminiferal Mg/Ca ratios. *Nature* **405**, 442–445 (2000).

59. Jonkers, L., Jim,nez-Amat, P., Mortyn, P. G. & Brummer, G.-J. A. Seasonal Mg/Ca variability of *N. pachyderma* (s) and *G. bulloides*: implications for seawater temperature reconstruction. *Earth Planet. Sci. Lett.* **376**, 137–144 (2013).

60. Hönisch, B. et al. The influence of salinity on Mg/Ca in planktic foraminifers - evidence from cultures, core-top sediments and complementary δ18O. *Geochim. Cosmochim. Acta* **121**, 196–213 (2013).

61. Gray, W. R. et al. The effects of temperature, salinity, and the carbonate system on Mg/Ca in Globigerinoides ruber (white): a global sediment trap calibration. *Earth Planet. Sci. Lett.* **482**, 607–620 (2018).

62. Evans, D., Wade, B. S., Henehan, M. J., Erez, J. & Müller, W. Revisiting carbonate chemistry controls on planktic foraminifera Mg/Ca: implications for sea surface temperature and hydrology shifts over the Paleocene–Eocene Thermal Maximum and Eocene–Oligocene transition. *Clim. Past.* **12**, 819–835 (2016).

63. Regenberg, M., Regenberg, A., Garbe-Schönberg, D. & Lea, D. W. Global dissolution effects on planktonic foraminiferal Mg/Ca ratios controlled by the calcite-saturation state of bottom waters. *Paleoceanography* **29**, 127–142 (2014).

64. Yu, J., Thornalley, D. J. R., Rae, J. W. B. & McCave, N. I. Calibration and application of B/Ca, Cd/Ca, and δ11B in *Neogloboquadrina pachyderma* (sinistral) to constrain CO₂ uptake in the subpolar North Atlantic during the last deglaciation. *Paleoceanography* **28**, 237–252 (2013).

65. Henehan, M. J. et al. A new boron isotope-pH calibration for *Orbulina universa*, with implications for understanding and accounting for 'vital effects'. *Earth Planet. Sci. Lett.* **454**, 282–292 (2016).

66. Henehan, M. J. et al. Calibration of the boron isotope proxy in the planktonic foraminifera *Globigerinoides ruber* for use in palaeo-CO₂ reconstruction. *Earth Planet. Sci. Lett.* **364**, 111–122 (2013).

67. Foster, G. L., Pogge von Strandmann, P. A. E. & Rae, J. W. B. Boron and magnesium isotopic composition of seawater. *Geochem. Geophys. Geosyst.* **11**, Q08015 (2010).

68. Klochko, K., Kaufman, A. J., Yao, W., Byrne, R. H. & Tossell, J. A. Experimental measurement of boron isotope fractionation in seawater. *Earth Planet. Sci. Lett.* **248**, 276–285 (2006).

69. Zeebe, R. E. & Wolf-Gladrow, D. A. *CO₂ in Seawater: Equilibrium, Kinetics, Isotopes* (Elsevier Oceanography Series, Amsterdam, 2001).

70. Adkins, J. F., McIntyre, K. & Schrag, D. P. The salinity, temperature, and δ18O of the glacial deep ocean. *Science* **289**, 1769–1773 (2002).

71. Lambeck, K., Rouby, H., Purcell, A., Sun, Y. & Sambridge, M. Sea level and global ice volumes from the Last Glacial Maximum to the Holocene. *Proc. Natl Acad. Sci. USA* **111**, 15296–15303 (2014).

72. Edgar, K. M., Anagnostou, E., Pearson, P. N. & Foster, G. L. Assessing the impact of diagenesis on δ11B, δ13C, δ18O, Sr/Ca and B/Ca values in fossil planktic foraminiferal calcite. *Geochim. Cosmochim. Acta* **166**, 189–209 (2015).

73. Hain, M. P., Sigman, D. M. & Haug, G. H. Carbon dioxide effects of Antarctic stratification, North Atlantic Intermediate Water formation, and subantarctic nutrient drawdown during the last ice age: diagnosis and synthesis in a geochemical box model. *Glob. Biogeochem. Cycles* **24**, GB4023 (2010).

74. Gattuso, J.-P. et al. Seacarb: Seawater Carbonate Chemistry with R. R package v.3.1.2 (CRAN, 2017); https://cran.r-project.org/web/packages/seacarb/seacarb.pdf

75. Millero, F. J. et al. Dissociation constants of carbonic acid in seawater as a function of salinity and temperature. *Mar. Chem.* **100**, 80–94 (2006).

76. Dickson, A. G. Standard potential of the reaction: AgCl(s) + 1/2H₂(g) = Ag(s) + HCl(aq), and the standard acidity constant of the ion HSO₄⁻ in synthetic sea water from 273.15 to 318.15 K. *J. Chem. Thermodyn.* **22**, 113–127 (1990).

77. Dickson, A. G. & Riley, J. P. The estimation of acid dissociation constants in seawater media from potentionmetric titrations with strong base. I. The ionic product of water - Kw. *Mar. Chem.* **7**, 89–99 (1979).

78. Ezat, M. M., Rasmussen, T. L., Honisch, B., Groeneveld, J. & deMenocal, P. Episodic release of CO₂ from the high-latitude North Atlantic Ocean during the last 135kyr. *Nat. Commun.* **8**, 14498 (2017).

79. Riethdorf, J.-R., Max, L., Nürnberg, D., Lembke-Jene, L. & Tiedemann, R. Deglacial development of (sub) sea surface temperature and salinity in the subarctic northwest Pacific: implications for upper-ocean stratification. *Paleoceanography* **28**, 91–104 (2013).

80. Seki, O. et al. Reconstruction of paleoproductivity in the Sea of Okhotsk over the last 30 kyr. *Paleoceanography* **19**, PA1016 (2004).

81. Seki, O. et al. Large changes in seasonal sea ice distribution and productivity in the Sea of Okhotsk during the deglaciations. *Geochem. Geophys. Geosyst.* **10**, Q10007 (2009).

82. Ganeshram, R. S., Pedersen, T. F., Calvert, S. E., McNeill, G. W. & Fontugne, M. R. Glacial-interglacial variability in denitrification in the worldas oceans: Causes and consequences. *Paleoceanography* **15**, 361–376 (2000).

83. Brunelle, B. G. et al. Evidence from diatom-bound nitrogen isotopes for subarctic Pacific stratification during the last ice age and a link to North Pacific denitrification changes. *Paleoceanography* **22**, PA1215 (2007).

84. Ito, T. & Follows, M. J. Preformed phosphate, soft tissue pump and atmospheric CO₂. *J. Mar. Res.* **63**, 813–839 (2005).

85. Talley, L. D. Closure of the global overturning circulation through the Indian, Pacific, and Southern Oceans: schematics and transports. *Oceanography* **86**(1), 80–97 (2013).

86. Peterson, C. D., Lisiecki, L. E. & Stern, J. V. Deglacial whole-ocean δ13C change estimated from 480 benthic foraminiferal records. *Paleoceanography* **29**, 549–563 (2014).

87. Otto-Bliesner, B. L. et al. Climate sensitivity of moderate-and low-resolution versions of CCSM3 to preindustrial forcings. *J. Clim.* **19**, 2567–2583 (2006).

88. Otto-Bliesner, B. L. et al. Last Glacial Maximum and Holocene climate in CCSM3. *J. Clim.* **19**, 2526–2544 (2006).